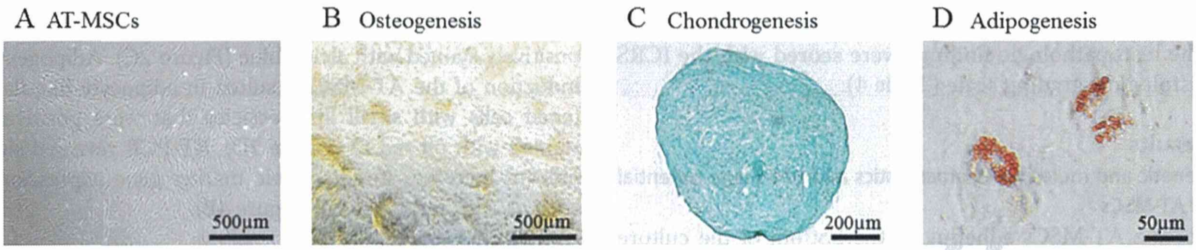

Figure 2 Representative images of special staining and RT-PCR results of tri-lineage differentiation in AT-MSCs. AT-MSCs adhering to the bottom of the culture dish were spindle-shaped **(A)**. Following 2 weeks of osteogenic induction, MSCs also showed characteristics of the stroma, including staining with alizarin red, indicating the presence of calcium apatite crystals **(B)**. Observation of the cell pellets that were induced by chondrogenic induction medium for 2 weeks showed a cartilage-like structure that was positively stained with alcian blue **(C)**. Adipogenic induction of the MSCs resulted in adipocyte-like flattened cells with small lipid vesicles that stained positively with oil red O **(D)**.

at 12 months after surgery. On the other hand, in the control site, a radiopaque area emerged in the shallow layer, but bone formation was not completed in the deep layer. The maximum diameter of the radiolucent area in the implanted site diminished in a stepwise manner and became 0 mm at 12 months after surgery. The control site remained at a diameter of 2.5 mm.

Macroscopic appearance and histopathology of the osteochondral defects

Macroscopic examination of animal no. 1 revealed that the surface of the implanted defect was covered with
F6 abundant cartilaginous white tissue (Figure 6A), while cartilaginous tissue was scarce and the surface was depressed in the control site (Figure 6B). Similarly, in animal no. 2, the surface was quite uniformly covered with abundant cartilaginous white tissues and the boundary to the surrounding normal cartilage was unclear in the implanted site (Figure 6C), compared with the findings at the control site (Figure 6D). The average macroscopic scores for the implanted site were higher than those for the control site in animal no. 1, while the differences between the scores for the implanted site and the control site were decreased in animal no. 2 (Table 3).

Histopathological sections of animal no. 1 at 6 months after surgery showed that thickened fibrocartilage had developed over the subchondral bone that was regenerating in the implanted site (Figure 7A, B). The surface of the F7
cartilage was smooth, and the boundary with the surrounding normal cartilage was obscure at the implanted site (Figure 7A). Meanwhile, the surface was collapsed and irregular at the control site (Figure 7C, D). The fibrocartilage showed more intense alcian blue staining and Col-II immunostaining at the implanted site (Figure 7E, F) compared with the control site (Figure 7G, H). In animal no. 2 at 12 months after surgery, partially thickened fibrocartilage was mounted on developed subchondral bone at the implanted site (Figure 7I, J). The surface of the cartilage was smooth, and the boundary with the surrounding normal cartilage was obscure, although small areas of endochondral ossification persisted at the center, and small amounts of AT had differentiated at the bottom part of the site (Figure 7I). Subchondral bone was symmetrically reconstructed in the defect and was covered by a mixed matrix of hyaline cartilage and fibrocartilage, in which clusters and columnar clusters of cells were observed (Figure 7J). In the control site, fibrocartilage had immediately covered the defect, but the subchondral ossification was poor (Figure 7K, L). The hyaline cartilage showed more intense and uniform alcian blue staining and Col-II immunostaining at the implanted site (Figure 7M, N) compared with the control site (Figure 7O, P). The averages of histologic scores for the implanted site were distinctly higher than those for the control site in both animals (Table 4).

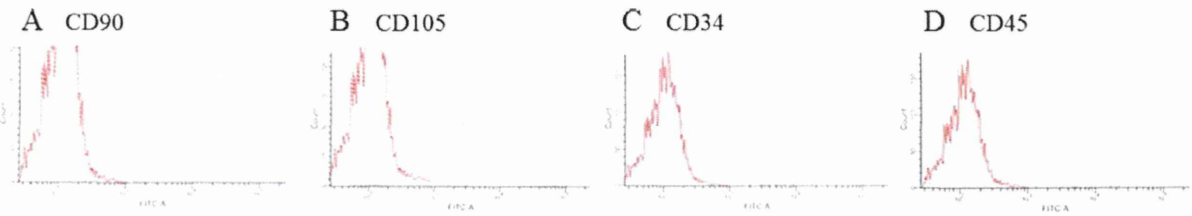

Figure 3 Flow cytometry results of immunological markers in AT-MSCs. A strong shift in MFI was detected with antibodies against CD90 **(A)** and CD105 **(B)**, whereas no signal reaction was detected with antibodies against CD34 **(C)** and CD45 **(D)**.

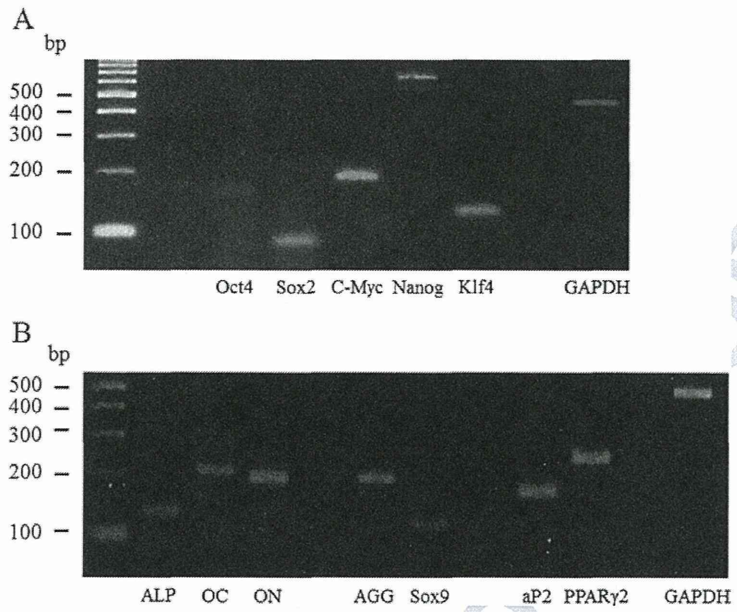

Figure 4 RT-PCR results of gene expression in AT-MSCs. Premature gene expression in AT-MSCs **(A)** and specific marker gene expression in AT-MSCs induced by tri-lineage differentiation medium **(B)** were confirmed.

Discussion

Human AT-MSCs have been shown to be positive for CD90, which suppresses the cancerization of stem cells [34], and CD105, which is associated with cellular responses to blood vessel formation and TGF-β1 [34]. The porcine AT-derived and spindle-shaped cells adhering to the bottom of the culture dish in the present study were strongly positive for CD90 and CD105. CD34, which is involved in cell adhesion and is expressed in hematopoietic stem cells [34], and CD45, which activates T and B lymphocyte receptors in hematopoietic cells [34], were both negative in the porcine AT-derived cells. Because human hematopoietic cells, but not human MSCs, were positive for these molecules [35,36], the porcine AT-derived cells may not be contaminated with hematopoietic cells [37]. Genetic markers specific for human MSCs, such as

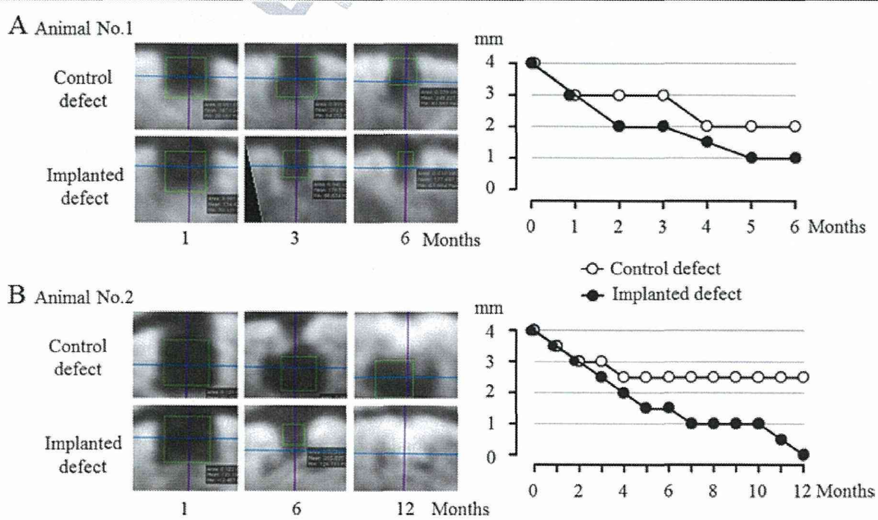

Figure 5 CT assessment of osteochondral defects. The upper image shows one cross section of the multiplanar reconstruction images 1, 3, and 6 months after the surgery in animal no. 1 **(A)**. The lower image shows one cross section of the multiplanar reconstruction images 1, 6, 12 months after the surgery in animal no. 2 **(B)**.

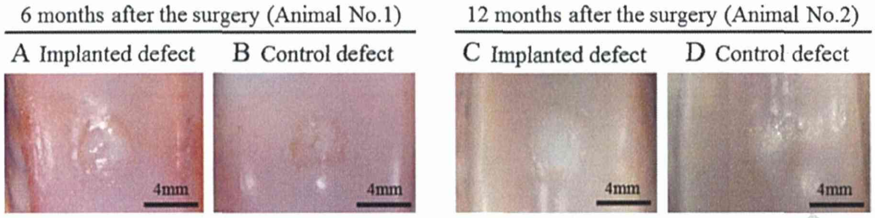

Figure 6 Macroscopic findings of the surface of the implanted and control sites. In animal no. 1, the surface of the implanted defect was covered with the abundant cartilaginous white tissues **(A)**, whereas the cartilaginous tissue was scarce and the surface was depressed in the control site **(B)**. In animal no. 2, the surface was more uniformly covered with abundant cartilaginous white tissues and the boundary to the surrounding normal cartilage was unclear in the implanted site **(C)**, comparing to those of the control site **(D)**.

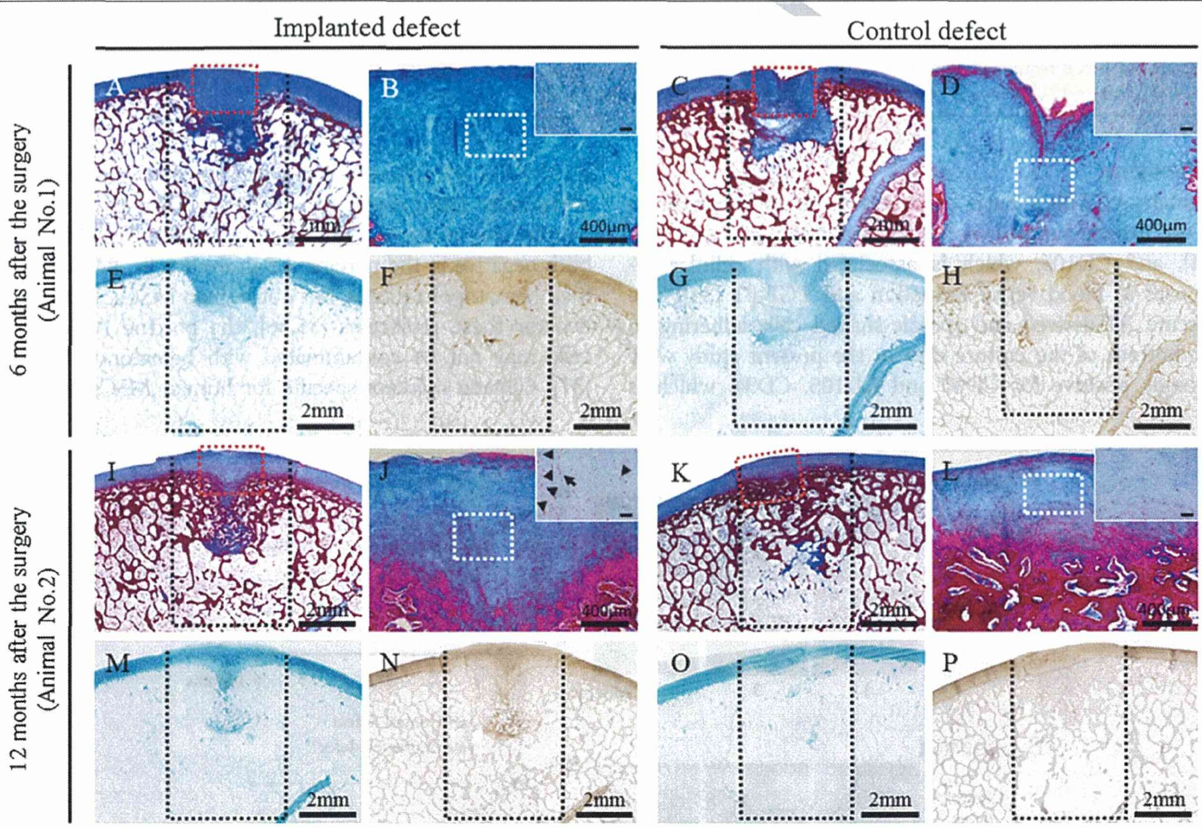

Figure 7 Histopathology of osteochondral defects using Masson's trichrome, alcian blue, and immunohistochemical staining of type II collagen. In animal no. 1, the articular surface was smooth and fibrocartilage developed on the subchondral bone at the implanted site **(A, B, E, F)**, whereas the surface was irregular and fibrous tissue lay over the subchondral bone at the control site **(C, D, G, H)**. At the implanted site in animal no. 2, the subchondral bone was symmetrically reconstructed and was covered by matrix including hyaline cartilage, which was suggested by the clusters (arrowhead) and columnar clusters (arrow) of cells **(I, J, M, N)**. On the other hand, smooth and continuous surface was restored due to fibrocartilage formation, but subchondral bone was absent in the bottom half of the defect, at the control site in animal no. 2 **(K, L, O, P)**. Black dotted lines indicate the areas of osteochondral defects immediately after the surgery. Masson's trichrome staining sections **(B, D, J, L)** were enlarged from red dotted square in the images **A**, **C**, **I**, and **K**, respectively. The insert images in sections **B**, **D**, **J**, and **L** were enlarged from white dotted square in images **B**, **D**, **J**, and **L**, respectively. The bars in the insert images indicate 50 μm.

SOX-2, OCT-4, NANOG [38], KLF-4, and C-MYC [39], were detected in the porcine cells by RT-PCR [40]. Moreover, the osteogenic, chondrogenic, and adipogenic potential of the cells was confirmed, and we therefore defined them as porcine AT-MSCs.

In accordance with a previously described procedure [21,33], we constructed scaffold-free 3D implants (diameter: 4 mm; height: 6 mm) composed of 760 spheroids each containing 5×10^4 autologous AT-MSCs. The cross-sectional CT images obtained at 6 and 12 months after implantation in animal no. 1 and animal no. 2, respectively, may mirror the histology because the localization, size, and shape of the radiolucent and radiopaque areas entirely corresponded with those of the fibrocartilage and regenerated bone. To further discriminate between cartilaginous and fibrous tissues in the radiolucent area, magnetic resonance imaging should be used.

The higher average macroscopic scores may suggest better improvement in superficial features at the implanted site, compared with the control site (Table 3). However, the differences in the average scores between the control and implanted sites were lower in animal no. 2 (euthanized at 12 months after surgery) than in animal no. 1 (euthanized at 6 months after surgery). All four features in the ICRS gross grading scale system were improved at the implanted site compared with the control defect site in animal no. 1, whereas a difference in neocartilage color only was seen between the two sites in animal no. 2. The results in animal no. 2 were not consistent with a previous study using rabbits, in which a more degraded macroscopic appearance of the control defect (diameter: 4.8 mm; depth: 5 mm) was observed at 12 months after implantation [21]. Based on the results, we speculate that the superficial features may improve spontaneously from 6 to 12 months after surgery for this size of osteochondral defect (diameter: 4 mm; depth: 6 mm) in MMPigs. To discriminate the superficial features caused by spontaneous repair from those caused by MSC-based regeneration in this size of defect, further evaluation of the pathology at 6 months after surgery will be appropriate in MMPigs. Other studies are needed to determine methods for repairing osteochondral defects with larger diameters and depths, which could never repair by themselves (as shown in the Additional files 1 and 2).

We also obtained higher average histologic scores at the implanted sites in both animals, which may indicate desirable osteochondral recovery compared with the control site (Table 4). As summarized in Table 5, regarding the histological features in animal no. 1, a smooth and continuous surface was restored by thickened fibrocartilage at the implanted site, whereas the surface was collapsed and irregular at the control site. Fibrocartilage formation and endochondral ossification during the process of MSC-based regeneration were present at the implanted site, compared with fibrous granulation matrix and inadequate bone formation in the control defect. On the other hand, in animal no. 2, a smooth and continuous articular surface was restored through cartilage formation at both sites, but subchondral bone formation was distinctly more satisfactory at the implanted site than at the control site, in which the trabecular pattern was completely absent (bone was detached) in the bottom half of the defect. Subchondral bone was covered by a mixed matrix of hyaline cartilage and fibrocartilage at the implanted site, while fibrocartilage had immediately covered the defect at the control site. These findings were similar to data reported previously reported in rabbits [21] and may suggest transformation of fibrocartilage into hyaline cartilage during the process of MSC-based osteocartilage regeneration. Because neither hyaline cartilage nor cell clusters were seen in the implanted defect site in animal no. 1, transformation of fibrocartilage into hyaline cartilage may begin between 6 and 12 months after implantation. However, more time may be required to regenerate pure, high-quality hyaline cartilage as well as complete subchondral regeneration in the implanted defect.

Consistent with a previous study on rabbits [21], we report here the successful outcome of osteochondral regeneration with scaffold-free AT-MSC constructs in MMPigs. Although further studies will be required, we conclude that implantation of a scaffold-free 3D construct of AT-MSCs into an osteochondral defect can regenerate the original structure of the bone and cartilage.

Conclusions

This pilot study suggests that implantation of a scaffold-free 3D construct of AT-MSCs into an osteochondral defect can induce regeneration of the original structure of the cartilage and subchondral bone over the course of 1 year.

Table 5 Summary of histological features

		Animal no. 1		Animal no. 2	
		Control site	Implanted site	Control site	Implanted site
Cartilage	Surface	Irregularity	Smooth	Smooth	Smooth
	Matrix	Fibrous tissue	Fibrocartilage	Fibrocartilage	Mixture; hyaline/fibrocartilage (transformation)
Subchondral bone		Granulation tissue	Increased remodeling	Detached (in the bottom half of the defect)	Increased remodeling (endochondral ossification)

Additional files

Additional file 1: Surgical procedure, CT images, macroscopic findings of the articular surface, and histopathology of osteochondral defects in animal no. 3. Figure S1. surgical procedure: A columnar construct (6 mm in diameter and 8 mm in height) composed of about 1,150 spheroids of AT-MSCs (A). An elliptic cylindrical osteochondral defect in each groove (B). Two constructs were autografted into the defect of the right hind limb (C). No implantation was in the left limb (B). **Figure S2.** CT images after the surgery: One cross section of the multi-planar reconstruction images 1, 6, and 12 months after the surgery in animal no. 3. In the implanted site, the radiopaque area gradually progressed and filled throughout the osteochondral defect after 12 months. However, in the control site, the spread of the radiopaque area was limited in the shallow layer, and no bone formation was in the deep layer. **Figure S3.** macroscopic findings of the articular surface: The surface was completely covered with abundant cartilaginous white tissues. The boundary to the surrounding normal cartilage was not different between the implanted site (A) and the control site (B). **Figure S4.** histopathology of osteochondral defects: At the implanted site, the restored subchondral bone was covered by mixture of hyaline/fibrocartilage, in which the clusters (arrowhead) and columnar clusters (arrow) of the cells were seen (A, B, C, D). In the control site, the surface was irregular, and the large fibrous tissue was presented in the subchondral (area with no bone at the bottom half of the defect (E, F, G, H)). Black dotted lines indicate the areas of osteochondral defects immediately after the surgery. Images B and F are high-power fields of the red dotted square in images A and E, respectively. The small images in sections B and F are high-power fields of white dotted squares in the respective images. The bars in the small images indicate 50 μm.

Additional file 2: ICRS gross grading scale and histological grading scale in animal no. 3. Table S1. ICRS gross grading scale. **Table S2.** ICRS histological grading scale.

Abbreviations

AGG: Aggrecan; ALP: Alkaline phosphatase; AP2: Adipocyte fatty acid-binding protein 2; AT: Adipose tissue; AT-MSCs: Adipose tissue-derived mesenchymal stem cells; BM: Bone marrow; BM-MSCs: Bone marrow-derived mesenchymal stem cells; CCM: Complete culture medium; C-MYC: Cellular myelocytomatosis oncogene; Col-II: Collagen type II; CT: Computed tomography; DMEM: Dulbecco's modified Eagle's medium; EDTA: Ethylenediaminetetraacetate; FACS: Fluorescence-activated cell sorting; FBS: Fetal bovine serum; KLF-4: Krüppel-like factor 4; MFI: Mean fluorescence intensity; MMPigs: Microminipigs; MSCs: Mesenchymal stem cells; NANOG: Homeobox protein NANOG; NBF: Neutral buffered formalin; TGF-β3: Transforming growth factor beta 3; OA: Osteoarthritis; OC: Osteocalcin; OCT-4: Octamer-binding transcription factor 4; ON: Osteonectin; PBS: Phosphate-buffered saline; PPAR-γ2: Peroxisome proliferator-activated receptor γ2; SB: Staining buffer; SOX-2: Sex-determining region Y box 2; SOX-9: Sex-determining region Y-box 9.

Competing interests

KN is a co-founder of Cyfuse Biomedical K.K. TT is a full-time employee of the same company. The other authors have no commercial, proprietary, or financial interest in the products or companies described in this article.

Authors' contributions

DM isolated and expanded AT-MSCs and performed genetic and molecular analysis. ST assessed the osteochondral defects by CT. TT prepared 3D constructs of AT-MSCs. HK assessed histopathologically. NM supervised histopathological assessment. MF implanted 3D constructs of AT-MSCs. KN conceived this study and interpreted the data. KM designed this experiment and interpreted the data. All authors approved the final version of the manuscript.

Acknowledgements

This study was supported by Japan Society for the Promotion of Science (grant no. 23380185 to KM). The study sponsor had no involvement in this study design, collection, analysis, or interpretation of data; in the writing of the manuscript; or in the decision to submit the manuscript for publication.

Author details

[1]Veterinary Surgery, Department of Veterinary Clinical Science, Joint Faculty of Veterinary Medicine, Kagoshima University, 21-24 Korimoto 1-chome, Kagoshima 890-0065, Japan. [2]Veterinary Teaching Hospital, Joint Faculty of Veterinary Medicine, Kagoshima University, 21-24 Korimoto 1-chome, Kagoshima 890-0065, Japan. [3]Cyfuse Biomedical K.K., 1-1 Maidashi 3-chome, Higashi-ku, Fukuoka 812-8582, Japan. [4]Veterinary Pathology, Department of Pathological and Preventive Sciences, Joint Faculty of Veterinary Medicine, Kagoshima University, 21-24 Korimoto 1-chome, Kagoshima 890-0065, Japan. [5]Department of Advanced Technology Fusion, Graduate School of Science and Engineering, Saga University, Honjyo 1-chome, Honjyo-cho, Saga 840-8502, Japan.

Received: 25 August 2014 Accepted: 25 February 2015

References

1. Muraki S, Oka H, Akune T, Mabuchi A, En-Yo Y, Yoshida M, et al. Prevalence of radiographic knee osteoarthritis and its association with knee pain in the elderly of Japanese population-based cohorts: the ROAD study. Osteoarthr Cartil. 2009;17:1137–43.
2. Gelber AC, Hochberg MC, Mead LA, Wang NY, Wigley FM, Klag MJ. Joint injury in young adults and risk for subsequent knee and hip osteoarthritis. Ann Intern Med. 2000;133:321–8.
3. Fernandes JC, Martel-Pelletier J, Pelletier JP. The role of cytokines in osteoarthritis pathophysiology. Biorheology. 2002;39:237–46.
4. Ding C, Cicuttini F, Scott F, Cooley H, Boon C, Jones G. Natural history of knee cartilage defects and factors affecting change. Arch Intern Med. 2006;166:651–8.
5. Muraki S, Akune T, Oka H, Mabuchi A, En-Yo Y, Yoshida M, et al. Association of occupational activity with radiographic knee osteoarthritis and lumbar spondylosis in elderly patients of population-based cohorts: a large-scale population-based study. Arthritis Rheum. 2009;61:779–86.
6. Mankin HJ. The response of articular cartilage to mechanical injury. J Bone Joint Surg Am. 1982;64:460–6.
7. Lane JG, Massie JB, Ball ST. Follow-up of osteochondral plug transfers in a goat model: a 6-month study. Am J Sports Med. 2004;32:1440–50.
8. Szerb I, Hangody L, Duska Z, Kaposi NP. Mosaicplasty: long-term follow-up. Bull Hosp Jt Dis. 2005;63:54–62.
9. Bentley G, Biant LC, Carrington RW, Akmal M, Goldberg A, Williams AM, et al. A prospective, randomised comparison of autologous chondrocyte implantation versus mosaicplasty for osteochondral defects in the knee. J Bone Joint Surg (Br). 2003;85:223–30.
10. Fujisato T, Sajiki T, Liu Q, Ikada Y. Effect of basic fibroblast growth factor on cartilage regeneration in chondrocyte-seeded collagen sponge scaffold. Biomaterials. 1996;17:155–62.
11. Funayama A, Niki Y, Matsumoto H, Maeno S, Yatabe T, Morioka H, et al. Repair of full-thickness articular cartilage defects using injectable type II collagen gel embedded with cultured chondrocytes in a rabbit model. J Orthop Sci. 2008;13:225–32.
12. Diaz-Romero J, Gaillard JP, Grogan SP, Nesic D, Trub T, Mainil-Varlet P. Immunophenotypic analysis of human articular chondrocytes: changes in surface markers associated with cell expansion in monolayer culture. J Cell Physiol. 2005;202:731–42.
13. Tatebe M, Nakamura R, Kagami H, Okada K, Ueda M. Differentiation of transplanted mesenchymal stem cells in a large osteochondral defect in rabbit. Cytotherapy. 2005;7:520–30.
14. Pittenger MF, Mackay AM, Beck SC, Jaiswal RK, Douglas R, Mosca JD, et al. Multilineage potential of adult human mesenchymal stem cells. Science. 1999;284:143–7.
15. Zuk PA, Zhu M, Ashjian P, De-Ugarte DA, Huang JI, Mizuno H, et al. Human adipose tissue is a source of multipotent stem cells. Mol Bio Cell. 2002;13:4279–95.
16. Gurevitch O, Slavin S, Resnick I, Khitrin S, Feldman A. Mesenchymal progenitor cells in red and yellow bone marrow. Folia Biol. 2009;55:27–34.
17. Stolzing A, Jones E, McGonagle D, Scutt A. Age-related changes in human bone marrow-derived mesenchymal stem cells: consequences for cell therapies. Mech Ageing Dev. 2008;129:163–73.
18. Asumda FZ, Chase PB. Age-related changes in rat bone-marrow mesenchymal stem cell plasticity. BMC Cell Biol. 2011;12:44.
19. Zuk PA, Zhu M, Mizuno H, Huang J, Futrell JW, Katz AJ, et al. Multilineage cells from human adipose tissue: implications for cell-based therapies. Tissue Eng. 2001;7:211–28.
20. Nakamura T, Sekiya I, Muneta T, Hatsushika D, Horie M, Tsuji K, et al. Arthroscopic, histological and MRI analyses of cartilage repair after a

minimally invasive method of transplantation of allogeneic synovial mesenchymal stromal cells into cartilage defects in pigs. Cytotherapy. 2012;14:327–38.

21. Ishihara K, Nakayama K, Akieda S, Matsuda S, Iwamoto Y. Simultaneous regeneration of full-thickness cartilage and subchondral bone defects in vivo using a three-dimensional scaffold-free autologous construct derived from high-density bone marrow-derived mesenchymal stem cells. J Orthop Surg Res. 2014;9:98.
22. Lu Z, Doulabi BZ, Huang C, Bank RA, Helder MN. Collagen type II enhances chondrogenesis in adipose tissue-derived stem cells by affecting cell shape. Tissue Eng Part A. 2010;16:81–90.
23. Yoon IS, Chung CW, Sung JH, Cho HJ, Kim JS, Shim WS, et al. Proliferation and chondrogenic differentiation of human adipose-derived mesenchymal stem cells in porous hyaluronic acid scaffold. J Biosci Bioeng. 2011;112:402–8.
24. Arrigoni E, De-Girolamo L, Di-Giancamillo A, Stanco D, Dellavia C, Carnelli D, et al. Adipose-derived stem cells and rabbit bone regeneration: histomorphometric, immunohistochemical and mechanical characterization. J Orthop Sci. 2013;18:331–9.
25. Park CW, Rhee YS, Park SH, Danh SD, Ahn SH, Chi SC, et al. In vitro/in vivo evaluation of NCDS-micro-fabricated biodegradable implant. Arch Pharm Res. 2010;33:427–32.
26. Koga H, Shimaya M, Muneta T, Nimura A, Morito T, Hayashi M, et al. Local adherent technique for transplanting mesenchymal stem cells as a potential treatment of cartilage defect. Arthritis Res Ther. 2008;10:R84.
27. Dashtdar H, Rothan HA, Tay T, Ahmad RE, Ali R, Tay LX, et al. A preliminary study comparing the use of allogenic chondrogenic pre-differentiated and undifferentiated mesenchymal stem cells for the repair of full thickness articular cartilage defects in rabbits. J Orthop Res. 2011;29:1336–42.
28. Lee JI, Sato M, Kim HW, Mochida J. Transplantation of scaffold-free spheroids composed of synovium-derived cells and chondrocytes for the treatment of cartilage defects of the knee. Eur Cell Mater. 2011;22:275–90.
29. Yoshioka T, Mishima H, Kaul Z, Ohyabu Y, Sakai S, Ochiai N, et al. Fate of bone marrow mesenchymal stem cells following the allogeneic transplantation of cartilaginous aggregates into osteochondral defects of rabbits. J Tissue Eng Regen Med. 2011;5:437–43.
30. Suzuki S, Muneta T, Tsuji K, Ichinose S, Makino H, Umezawa A, et al. Properties and usefulness of aggregates of synovial mesenchymal stem cells as a source for cartilage regeneration. Arthritis Res Ther. 2012;14:R136.
31. Kawaguchi H, Miyoshi N, Miura N, Fujiki M, Horiuchi M, Izumi Y, et al. Microminipig, a non-rodent experimental animal optimized for life science research: novel atherosclerosis model induced by high fat and cholesterol diet. J Pharmacol Sci. 2011;115:115–21.
32. Takeishi K, Horiuchi M, Kawaguchi H, Deguchi Y, Izumi H, Arimura E, et al. Acupuncture improves sleep conditions of minipigs representing diurnal animals through an anatomically similar point to the acupoint (GV20) effective for humans. Evid Based Complement Alternat Med. 2012;2012:472982.
33. Nakayama K. In vitro biofabrication of tissues and organs. In: Forgacs G, Sun W, editors. Biofabrication: micro- and nano-fabrication, printing, patterning and assemblies. Oxford: William Andrew; 2013. p. 1–21.
34. Zola H, Swart B, Nicholson I, Voss E. Leukocyte and stromal cell molecules: the CD markers. Hoboken: John Wiley & Sons Inc; 2007.
35. Chen J, Lu Z, Cheng D, Peng S, Wang H. Isolation and characterization of porcine amniotic fluid-derived multipotent stem cells. PLoS One. 2011;6:e19964.
36. Guo KT, SchAfer R, Paul A, Gerber A, Ziemer G, Wendel HP. A new technique for the isolation and surface immobilization of mesenchymal stem cells from whole bone marrow using high-specific DNA aptamers. Stem Cells. 2006;10:2220–31.
37. Casado JG, Gomez-Mauricio G, Alvarez V, Mijares J, Tarazona R, Bernad A, et al. Comparative phenotypic and molecular characterization of porcine mesenchymal stem cells from different sources for translational studies in a large animal model. Vet Immunol Immunopathol. 2012;147:104–12.
38. Riekstina U, Cakstina I, Parfejevs V, Hoogduijn M, Jankovskis G, Muiznieks I, et al. Embryonic stem cell marker expression pattern in human mesenchymal stem cells derived from bone marrow, adipose tissue, heart and dermis. Stem Cell Rev. 2009;5:378–86.
39. Windmolders S, De-Boeck A, Koninckx R, Daniëls A, De-Wever O, Bracke M, et al. Mesenchymal stem cell secreted platelet derived growth factor exerts a pro-migratory effect on resident cardiac atrial appendage stem cells. J Mol Cell Cardiol. 2014;66:177–88.
40. Tang L, Yin Y, Zhou H, Song G, Fan A, Tang B, et al. Proliferative capacity and pluripotent characteristics of porcine adult stem cells derived from adipose tissue and bone marrow. Cell Reprogram. 2012;14:342–52.